Open access • Journal Article • DOI:10.1109/TMTT.1980.1130071

Methods of Efficiency Enhancement and Scaling for the Gyrotron Oscillator

Kwo Ray Chu, M. E. Read, A. K. Ganguly

Published on: 01 Apr 1980 - IEEE Transactions on Microwave Theory and Techniques (IEEE)

Methods of Efficiency Enhancement and Scaling for the Gyrotron Oscillator

KWO RAY CHU, MICHAEL E. READ, AND ACHINTYA K. GANGULY

Abstract—**It is shown that a gyrotron oscillator operating in a slightly tapered magnetic field can attain an efficiency of ~78 percent, approximately 1.7 times higher than that obtainable in a constant magnetic field. Extensive numerical data have been tabulated and a convenient parameter is introduced to generate numerical efficiency scaling relations through which optimum operating conditions are clearly exhibited. Conditions for reaching the high efficiency operating regime are also studied and numerically illustrated.**

I. Introduction

THE GYROTRON is a microwave device based on the cyclotron maser interaction between an electromagnetic wave and an electron beam in which the individual electrons move along helical trajectories in the presence of an applied magnetic field. In recent years, it has emerged as a new and by far the most powerful source of coherent millimeter and submillimeter radiation. Potential applications of the gyrotron include radar, communication, and plasma heating of controlled nuclear fusion devices. Most of the work on gyrotrons, both theoretical and experimental, has been carried out for two basic configurations: (i) the single cavity configuration, and (ii) the waveguide configuration. In the first configuration (the gyrotron oscillator), the electron beam sustains a constant amplitude normal mode oscillation in an open end cavity. In the second configuration (the gyrotron travelling wave amplifier), the electron beam amplifies the normal mode of a fast waveguide structure. A detailed analysis of the cyclotron maser mechanism [1] as well as review articles [2], [3] on the gyrotron development can be found in recent literature.

The present work proposes a method for enhancing the efficiency of gyrotron oscillators and studies the scaling of efficiency with respect to the operating parameters.

Our primary motivation for achieving a high-efficiency gyrotron is connected with its application in controlled fusion research. To reach the fusion ignition temperature, a great amount of energy (many megajoules) has to be injected for plasma heating. Furthermore, this should be done with the maximum efficiency in order to alleviate the energy breakeven condition. A highly efficient gyrotron has been recognized as one of the most promising sources to meet these requirements. Many methods for efficiency enhancement have so far been considered. These methods are largely variations of two general approaches. The first approach [4]–[13] involves the contouring of the wave electric field profile. The second approach [14], [15] also employed in the present paper, involves the contouring of the applied dc magnetic field. For a brief review of the previous results, two commonly used definitions of efficiency need to be distinguished. The overall efficiency (η) is defined as the average electron energy loss divided by its total initial energy and the transverse efficiency ($\eta_\perp$) is the same quantity divided by the initial transverse energy. Thus, $\eta \simeq 0.8\eta_\perp$ if $v_\perp/v_z = 2$, and $\eta \simeq 0.7\eta_\perp$ if $v_\perp/v_z = 1.5$. For a sinusoidal wave electric field profile, the maximum achievable efficiency (η) is approximately [16] 42 percent for $v_\perp/v_z = 2$ and 35 percent for $v_\perp/v_z = 1.5$. Using a Gaussian wave electric field profile and $v_\perp/v_z = 1.5$, Nasinovich *et al.* [5], [10] have shown that $\eta_\perp$ can reach 79 percent (or $\eta = 55$ percent). Using a more complicated (axially asymmetric) wave electric field profile, Kolosov and Kurayev [7] have calculated a maximum transverse efficiency of 88 percent. The above figures all refer to the fundamental cyclotron harmonic and uniform applied magnetic field. However, it has been shown in [7] and [10] that the maximum efficiency at the second cyclotron harmonic differs only slightly from that of the fundamental cyclotron harmonic. In practice, the wave electric field contouring can be achieved by contouring the cross section of the cavity [11], as is done by Kisel *et al.* [9]. In the case of applied magnetic-field contouring. Sprangle and Smith [15] proposed a method which employs a two-stage magnetic field. Except for a short transition region, the magnetic field is held constant in each stage. In the first stage, the magnetic field is below that required for strong resonant interaction, hence only electron bunching takes place. In the second stage, the magnetic field is raised to the value for strong interaction, thus allowing the bunched electrons to lose a substantial amount of energy. They have calculated a maximum transverse efficiency of 75 percent (or $\eta = 60$ for $v_\perp/v_z = 2$). Because of the presence of a bunching stage, a relatively longer cavity is required in their scheme. This may become a rather strong limiting factor in high-power operations.

In the present study a linearly tapered magnetic field is employed for the purpose of efficiency enhancement. The magnetic field increases uniformly over the length of the cavity with approximately a 10-percent variation from end

Manuscript received July 9, 1979; revised November 29, 1979. This work was supported by the U. S. Department of Energy under Contract EX-77-A-34-1015.

The authors are with the Naval Research Laboratory, Washington, DC 20375

to end. For $v_\perp/v_z = 1.5$, 2, and 2.5, we have calculated a maximum overall efficiency of 56, 67, and 78 percent, respectively (corresponding to $\eta_\perp = 80$, 84, and 90 percent, respectively). Compared with the other methods discussed above, this method promises a very high efficiency with the simplest structure.

As shown in a recent linear analysis [17] the nature of the cyclotron maser interaction in a cavity is much more complicated than that in a waveguide mainly because the electromagnetic wave in a cavity consists of both a forward and a backward component as compared with a single forward component in the waveguide. As a result, nonlinear analysis of the gyrotron oscillator, mainly the calculation of its efficiency, becomes difficult to treat analytically. Thus far, practically all the nonlinear analyses of gyrotron oscillators (including the present one) have been based on numerical computation. In comparison, the nonlinear analyses [18]–[20] of gyrotron travelling wave amplifiers have been more analytical in nature. While the numerical approach allows one to employ more exact physical models, it often fails to show the general properties of the system examined. This limitation has made it difficult to identify the optimum modes and parameters of operation from a great number of possibilities. Thus a second objective of the present paper is to seek from the extensive numerical data a simple efficiency scaling relation which clearly shows the optimum operating conditions. We found that there exists a common parameter N_c, i.e., the total number of cyclotron orbits executed by an electron in traversing the cavity, which connects the seemingly random data into smooth curves. Indeed, as the final result will indicate, N_c appears to be a convenient parameter for generating the common operating characteristics for gyrotron oscillators operating at different modes.

The paper is organized as follows: In Section II, we present the model, assumptions, and basic gyrotron equations; In Section III, the main results are obtained and a design example is given on the basis of the optimized data; In Section IV, we study the accessibility of the high-efficiency regime, a problem of considerable practical importance but not yet addressed theoretically; Section V contains further discussions and a brief description of the preliminary experimental results.

II. Model, Assumptions, and Basic Equations

Fig. 1(a) and (b) illustrate the single cavity gyrotron oscillator model under study. An annular electron beam is injected into an open-end cavity from the left hand side and propagates to the right under the guidance of an applied magnetic field $\boldsymbol{B}_0$ (Fig. 1(a)). The electrons, moving along helical trajectories, have a substantial part of their kinetic energy in the form of transverse motion. Inside the cavity, the electron beam gives up a portion of its energy through interaction with the EM fields. If the average power lost by the beam equals the wave power diffracted out of the cavity, a steady state is then established. A main objective of our calculation is to maximize the beam energy loss at the steady state. The electron

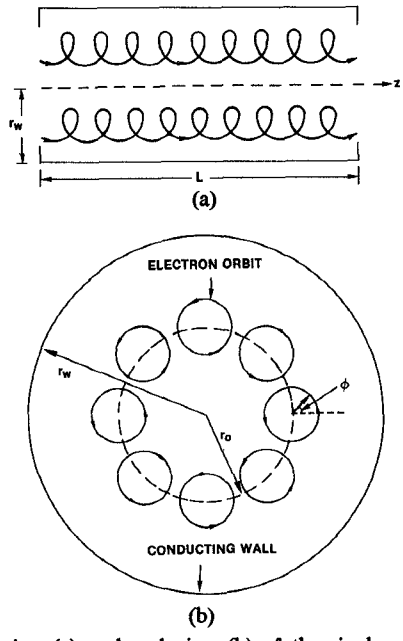

Fig. 1. Side view (a) and end view (b) of the single cavity gyrotron oscillator.

beam shown in Fig. 1 is typical of those generated from a magnetron-type electron gun. Both theory [21] and experiment [22] have shown that a beam so generated has the desirable properties for gyrotron applications, namely, it has the minimum spread in velocity and radial position. Thus, in our model we assume that the beam electrons are monoenergetic with their guiding centers located on the same surface of constant radius ($r = r_0$). Fig. 1(b) shows the cross-sectional view of the model. We assume further that the beam is sufficiently tenuous that its space charge field can be neglected and that it will not modify the normal mode EM field structure of the cavity. This is a good assumption for beam powers below a few hundred kilowatts. Since the cyclotron maser interaction takes place between the electron beam and the TE mode (rather than the TM mode) and axially symmetric TE modes (i.e., modes without azimuthal variations) have the smallest wall loss, we will limit our consideration to the TE_{0nl} modes, where n and l are, respectively, the radial and axial eigenmode numbers. Under these assumptions, the electron dynamics are governed by the following equation of motion:

$$\frac{d}{dt}\gamma m\boldsymbol{v} = -e(\boldsymbol{E} + \boldsymbol{v}\times\boldsymbol{B}) \tag{1}$$

where $\gamma = (1 - v^2/c^2)^{-\frac{1}{2}}$, $\boldsymbol{E} = E_\theta \boldsymbol{e}_\theta$, $\boldsymbol{B} = \boldsymbol{B}_0 + B_r\boldsymbol{e}_r + B_z\boldsymbol{e}_z$, $\boldsymbol{B}_0$ is the applied magnetic field (to be specified later), and E_θ, B_r, B_z are the TE_{0nl} wave fields given by

$$E_\theta = E_{\theta 0} J_1(k_n r) \sin k_z z \cos \omega t \tag{2}$$

$$B_r = (k_z/\omega) E_{\theta 0} J_1(k_n r) \cos k_z z \sin \omega t \tag{3}$$

$$B_z = -(k_n/\omega) E_{\theta 0} J_0(k_n r) \sin k_z z \sin \omega t \tag{4}$$

where $k_z = \pi l/L$, $k_n = x_n/r_w$, x_n is the nth nonvanishing root of $J_1(x) = 0$, $\omega = (k_z^2 + k_n^2)^{1/2} c$ is the wave frequency, and r_w is the inner radius of the cavity.

The total wave energy stored in the cavity (W_f) can be written,

$$W_f = 0.25\pi\epsilon_0 E_{\theta 0}^2 J_0^2(x_n) r_w^2 L$$

where $\epsilon_0 = (36\pi)^{-1}10^{-9}$ farad/m is the vacuum dielectric constant and $J_0^2(x_n) \simeq 0.16$, 0.09, 0.0625 for $n = 1$, 2, 3. If we assume that the quality factor Q of the cavity is entirely due to diffraction loss (i.e., neglecting wall loss), we obtain the wave power (P_w) emitted from the cavity

$$P_w = \omega W_f / Q$$
$$= 0.25\pi\epsilon_0 \omega E_{\theta 0}^2 J_0^2(x_n) r_w^2 L / Q. \quad (5)$$

Thus, the beam power (P_b) required to sustain a steady-state oscillation in the cavity is

$$P_b = P_w / \eta$$
$$= 0.25\pi\epsilon_0 \omega E_{\theta 0}^2 J_0^2(x_n) r_w^2 L / \eta Q \quad (6)$$

where η is the efficiency to be evaluated from (1).

It is convenient to introduce a normalization scheme by which the cavity radius r_w is scaled out of the equations. This can be achieved through the following procedures (normalized notations are denoted by a bar):

(i) length normalized to r_w ($\bar{r} = r/r_w$);
(ii) frequency normalized to c/r_w ($\bar{\omega} = \omega r_w / c$);
(iii) velocity normalized to c ($\bar{v} = v/c$); and
(iv) electric and magnetic field normalized to mc^2/er_w and mc/er_w, respectively ($\bar{E}_\theta = E_\theta e r_w / mc^2$, $\bar{B}_0 = B_0 e r_w / mc$).

Other quantities such as k_z and t are to be normalized consistently with the preceding procedures ($\bar{k}_z = k_z r_w$, $\bar{t} = tc/r_w$). However, naturally dimensionless quantities such as γ and η will remain unchanged. Results obtained under the normalized representation are thus applicable to cavities of arbitrary radius.

We may now rewrite (1)–(6) as

$$\frac{d}{d\bar{t}}\gamma m\bar{v} = -(\bar{E} + \bar{v} \times \bar{B}) \quad (7)$$

$$E_\theta = \bar{E}_{\theta 0} J_1(x_n \bar{r}) \sin \bar{k}_z \bar{z} \cos \bar{\omega} \bar{t} \quad (8)$$

$$\bar{B}_r = (\bar{k}_z / \bar{\omega}) \bar{E}_{\theta 0} J_1(x_n \bar{r}) \cos \bar{k}_z \bar{z} \sin \bar{\omega} \bar{t} \quad (9)$$

$$\bar{B}_z = -(x_n / \bar{\omega}) \bar{E}_{\theta 0} J_0(x_n \bar{r}) \sin \bar{k}_z \bar{z} \sin \bar{\omega} \bar{t} \quad (10)$$

$$QP_w = 548 \bar{\omega} \bar{E}_{\theta 0}^2 J_0^2(x_n) \bar{L}\ MW \quad (11)$$

$$QP_b = 548 \bar{\omega} \bar{E}_{\theta 0}^2 J_0^2(x_n) \bar{L} / \eta\ MW. \quad (12)$$

To obtain the efficiency from this set of equations, we solve (7) numerically for the energy loss (or gain) by a single electron in traversing the cavity. The efficiency is then evaluated by averaging over an ensemble of electrons uniformly distributed in their initial gyrational phase angle ϕ (Fig. 1(b)). In solving (7), the following initial conditions and parameters need to be specified: The initial electron energy (γ_0) and velocity ratio ($\alpha \equiv v_{\perp 0}/v_{z0}$), the initial electron guiding center position ($\bar{r}_0$), the cavity dimension ($\bar{L}$), the mode numbers (n and l), the wave field strength ($\bar{E}_{\theta 0}$), and the applied magnetic field profile

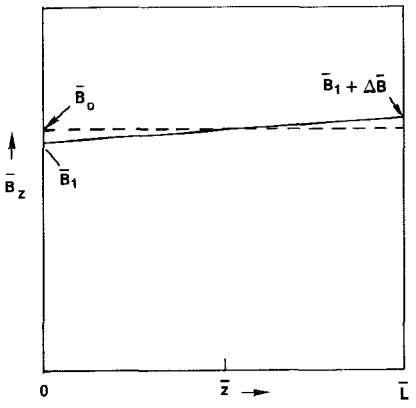

Fig. 2. Typical profile of the tapered magnetic field (solid line). For comparison, $\bar{B}_z$ profile of the constant magnetic field is also plotted in dashed line.

($\bar{B}_0$) defined below,

$$\bar{B}_0(\bar{r}, \bar{z}) = \bar{B}_{0r} e_r + \bar{B}_{0z} e_z \quad (13)$$

where

$$\bar{B}_{0r}(\bar{r}) = -\frac{1}{2}\Delta\bar{B}\bar{r}/\bar{L} \quad (14)$$

$$\bar{B}_{0z}(\bar{z}) = \bar{B}_1 + \Delta\bar{B}\bar{z}/\bar{L}. \quad (15)$$

Fig. 2 shows the axial magnetic field ($\bar{B}_{0z}$) profile inside the cavity. The variation of $\bar{B}_{0z}$ is typically in the neighborhood of 10 percent, hence $\bar{B}_0$ points predominantly in the z-direction. For comparison, we will also calculate the efficiency for a constant applied magnetic field, in which case $\bar{B}_0$ is simply

$$\bar{B}_0 = \bar{B}_0 e_z \quad (16)$$

where $\bar{B}_0$ is a constant.

The beam guiding center position for maximum coupling with the wave has been calculated in [17]. Here we will limit our consideration to the case of fundamental cyclotron harmonic interaction and $\bar{r}_0$ for maximum beam-wave coupling is given by [17],

$$\bar{r}_0 = 1.8/x_n \quad (17)$$

where $x_n = 3.8$, 7.0 and 10.2 for $n = 1$, 2, 3, respectively. To reduce the number of free parameters, we fix the electron energy at 70 keV. This is a voltage capable of generating a sufficiently high power electron beam for most applications presently conceived, including plasma heating of controlled fusion devices. The axial eigenmode number will be fixed at the lowest value ($l = 1$) because it gives the highest cavity Q and hence the lowest threshold beam power compared with the $l \neq 1$ modes. Thus the unwanted high l modes will not be excited if one operates near the threshold of the $l = 1$ mode. The remaining parameters, α, $\bar{L}$, n, $\bar{E}_{\theta 0}$, $\bar{B}_0$, $\bar{B}_1$, and $\Delta\bar{B}$ etc., will be varied.

III. Results

A typical data point is obtained as follows. We first specify α, $\bar{L}$, and n. In the case of tapered magnetic field,

TABLE I
OPTIMUM EFFICIENCY DATA FOR $\alpha = 1.5$ AND TAPERED MAGNETIC FIELD

Data No.	1	2	3	4	5	6
Mode	TE_{011}	TE_{011}	TE_{021}	TE_{031}	TE_{021}	TE_{031}
$\bar{L}$	5	8	5	5	8	8
$\bar{r}_0$	0.48	0.48	0.26	0.18	0.26	0.18
$\bar{\omega}$	3.88	3.85	7.04	10.19	7.03	10.18
$\bar{B}_1$	3.69	3.85	7.17	10.76	7.47	11.07
$\Delta\bar{B}$	0.85	0.57	0.85	0.61	0.34	0.27
$\bar{E}_{\theta 0}$	0.22	0.15	0.24	0.25	0.16	0.12
QP_b^{th} (MW)	69	54	109	500	687	∞
QP_b^{op} (MW)	210	126	194	195	126	85
QP_w (MW)	83	62	100	109	70	40
η^{op} (%)	39.5	48.9	51.6	55.7	55.4	46.9
N_c	10.7	17.4	20.0	29.2	32.1	47.2

TABLE II
OPTIMUM EFFICIENCY DATA FOR $\alpha = 1.5$ AND CONSTANT MAGNETIC FIELD

Data No.	7	8	9	10	11	12
Mode	TE_{011}	TE_{011}	TE_{021}	TE_{031}	TE_{021}	TE_{031}
$\bar{L}$	5	8	5	5	8	8
$\bar{r}_0$	0.48	0.48	0.26	0.18	0.26	0.18
$\bar{\omega}$	3.88	3.85	7.04	10.19	7.03	10.18
$\bar{B}_0$	4.08	4.16	7.60	11.13	7.66	11.22
$\bar{E}_{\theta 0}$	0.20	0.13	0.18	0.15	0.10	0.08
QP_b^{th} (MW)	95	41	100	172	746	∞
QP_b^{op} (MW)	241	127	159	113	85	68
QP_W (MW)	68	43	55	40	29	18
η^{op} (%)	28.2	33.5	34.9	34.5	33.7	26.1
N_c	10.7	17.4	20.0	29.2	32.1	47.2

TABLE III
OPTIMUM EFFICIENCY DATA FOR $\alpha = 2$ AND TAPERED MAGNETIC FIELD

Data No.	13	14	15	16	17
Mode	TE_{011}	TE_{011}	TE_{021}	TE_{031}	TE_{021}
$\bar{L}$	5	8	5	5	8
$\bar{r}_0$	0.48	0.48	0.26	0.18	0.26
$\bar{\omega}$	3.88	3.85	7.04	10.19	7.03
$\bar{B}_1$	3.83	3.96	7.34	10.93	7.58
$\Delta\bar{B}$	0.59	0.37	0.49	0.34	0.21
$\bar{E}_{\theta 0}$	0.19	0.14	0.22	0.18	0.11
QP_b^{th} (MW)	45	80	400	7580	∞
QP_b^{op} (MW)	109	81	126	96	62
QP_W (MW)	62	54	82	56	34
η^{op} (%)	57.2	67.1	66.6	58.5	54.2
N_c	13.4	21.5	24.7	36.5	40.1

TABLE IV
OPTIMUM EFFICIENCY DATA FOR $\alpha = 2$ AND CONSTANT MAGNETIC FIELD

Data No.	18	19	20	21	22
Mode	TE_{011}	TE_{011}	TE_{021}	TE_{031}	TE_{021}
$\bar{L}$	5	8	5	5	8
$\bar{r}_0$	0.48	0.48	0.26	0.18	0.26
$\bar{\omega}$	3.88	3.85	7.04	10.19	7.03
$\bar{B}_0$	4.13	4.14	7.61	11.22	7.70
$\bar{E}_{\theta 0}$	0.15	0 10	0.15	0.14	0.08
QP_b^{th} (MW)	50	85	250	∞	∞
QP_b^{op} (MW)	104	66	97	100	59
QP_W (MW)	40	27	39	34	18
η^{op} (%)	38.5	41.2	40.2	34.1	29.7
N_c	13.4	21.5	24.7	36.5	40.1

the efficiency η is then evaluated as a function of $\bar{E}_{\theta 0}$, $\bar{B}_1$, and $\Delta\bar{B}$. The point where $\eta(\bar{E}_{\theta 0}, \bar{B}_1, \Delta\bar{B})$ peaks will be taken as a data point and referred to as the optimum efficiency η^{op}. In the case of constant magnetic field, η is evaluated as a function of $E_{\theta 0}$ and $\bar{B}_0$, and similarly the peak of $\eta(\bar{E}_{\theta 0}, \bar{B}_0)$ becomes a data point.

As a check of the numerical accuracy, we monitor a constant of motion, the canonical angular momentum $\bar{P}_\theta (\equiv \gamma \bar{r} m v_\theta - \bar{r}\bar{A}_\theta$, where $\bar{A}_\theta$ is the vector potential of the EM fields). In all the numerical runs, $\bar{P}_\theta$ is found to fluctuate not more than 10^{-5}, an indication of good numerical accuracy.

Tables I, III, and V list the optimum efficiency data obtained for the tapered magnetic field profile. Each table applies to a fixed value of $\alpha (\equiv v_{\perp 0}/v_{z0})$, while entries in the same table are for various mode numbers (n) and cavity length ($\bar{L}$). For comparison, Tables II, IV, and VI list the corresponding optimum efficiency data obtained for a constant magnetic field profile. In Tables I through VI, QP_b^{op} is the product of the quality factor Q and the beam power at optimum efficiency operation. Similarly QP_b^{th} is Q times the threshold beam power required to start the oscillation under conditions optimized for efficiency. The significance of P_b^{th} will be discussed further in Section IV.

In all the data presented, we have kept track of a common parameter N_c, the total number of cyclotron orbits executed by a single electron in traversing the cavity. To illustrate the efficiency scaling with respect to N_c and the efficiency enhancement due to magnetic field tapering, we have plotted η^{op} against N_c in Fig. 3(a), (b), and (c). In these and all the subsequent figures, solid curves refer to the tapered magnetic field and dashed curves refer to the constant magnetic field. The lowest curves in Fig. 3(a), (b), and (c) give $\Delta\bar{B}/\bar{B}_1$, a measure of the magnetic field tapering (see Fig. 2). The numbered dots refer to the data number in Tables I through VI. Fig. 4 shows typical plots of efficiency versus the axial distance inside the cavity. It is seen that in both the tapered and constant magnetic field cases, strong interaction (as witnessed by the rapid rise of efficiency) takes place after an initial bunching stage. However, in a tapered magnetic field, the region of strong interaction stretches farther at both ends, resulting in higher efficiency.

TABLE V
OPTIMUM EFFICIENCY DATA FOR $\alpha = 2.5$ AND TAPERED MAGNETIC FIELD

Data No.	23	24	25	26	27	28
Mode	TE_{011}	TE_{011}	TE_{021}	TE_{011}	TE_{021}	TE_{021}
$\bar{L}$	4	6	4	8	5	6
$\bar{r}_o$	0.48	0.48	0.26	0.48	0.26	0.26
$\bar{\omega}$	3.91	3.87	7.06	3.85	7.04	7.04
$\bar{B}_1$	3.84	3.93	7.28	3.98	7.37	7.47
$\Delta\bar{B}$	0.61	0.44	0.61	0.30	0.45	0.30
$\bar{E}_{\theta o}$	0.20	0.16	0.26	0.14	0.22	0.16
QP_b^{th} (MW)	33	49	191	102	199	204
QP_b^{op} (MW)	82	72	123	69	108	74
QP_w (MW)	55	53	94	54	84	53
η^{op} (%)	67.0	73.5	76.5	77.8	77.5	72.2
N_c	12.9	19.5	23.9	26.2	30.1	36.2

TABLE VI
OPTIMUM EFFICIENCY DATA FOR $\alpha = 2.5$ AND CONSTANT MAGNETIC FIELD

Data No.	28	30	31	32	33	34
Mode	TE_{011}	TE_{011}	TE_{021}	TE_{011}	TE_{021}	TE_{021}
$\bar{L}$	4	6	4	8	5	6
$\bar{r}_o$	0.48	0.48	0.26	0.48	0.26	0.26
$\bar{\omega}$	3.91	3.87	7.06	3.85	7.04	7.04
$\bar{B}_o$	4.12	4.15	7.63	4.18	7.68	7.71
$\bar{E}_{\theta o}$	0.17	0.11	0.16	0.07	0.11	0.09
QP_b^{th} (MW)	58	50	102	45	133	336
QP_b^{op} (MW)	97	56	83	32	54	49
QP_w (MW)	40	25	36	13	21	17
η^{op} (%)	41.2	44.4	43.1	41.9	39.0	34.7
N_c	12.9	19.5	23.9	26.2	30.1	36.2

TABLE VII
DESIGN PARAMETERS OF A 35-GHZ GYROTRON OSCILLATOR-BASED ON DATA NUMBER 14 IN TABLE III

Mode	TE_{011}
beam voltage	70 kV
beam current	2.31 Amp
$v_{\perp 0}/v_{\parallel 0}$	2.0
cavity radius r_w	0.526 cm
cavity length L	4.208 cm
beam guiding center position r_0	0.252 cm
B_1	12.84 kG
ΔB	1.20 kG
efficiency η	67.1 %
Q	500
threshold beam power P_b^{th}	160.0 kW
optimum beam power P_b^{op}	162.0 kW
output wave power P_w	108.7 kW

On the basis of the data presented here, we may summarize the principal results as follows.

1) With magnetic field tapering, one can enhance the peak efficiency by a factor of 1.6 to 1.7 over what is obtainable in a constant magnetic field and the required amount of tapering ($\Delta\bar{B}/\bar{B}_1$) is only a few percent (Fig. 3). The higher the velocity ratio α, the higher the maximum achievable efficiency. The peak efficiencies for $\alpha = 1.5$, 2.0, and 2.5 as shown in Fig. 3 are, respectively, 34.9, 41.2, and 44.4 percent for the constant magnetic field and 55.7, 67.1, and 77.8 percent for the tapered magnetic field. Currently available electron beams have a maximum α value of ~ 2, hence a 67 percent efficiency can be achieved (in a tapered magnetic field) with the present technology. For the purpose of further efficiency enhancement, it is desirable to improve the electron gun design so that beams with higher α can be obtained.

2) N_c is shown to be a convenient scaling parameter for the efficiency for both the constant and tapered magnetic field cases (Fig. 3). We observe in Fig. 3 that for a fixed α, the efficiency data calculated for various modes (n) and cavity dimensions ($\bar{L}$) form a smooth curve when plotted against N_c. In other words, the efficiency is only a function of N_c regardless of the mode of operation and the dimension of the cavity. Thus, for modes and cavity dimensions not calculated here, one can predict its efficiency by simply calculating the value of N_c and interpolating from the data presented. Similarly, through this method of scaling, efficiency optimization for any given mode of operation becomes a simple task of specifying the cavity length such that N_c has the value corresponding to the peak efficiency in Fig. 3. In general, the efficiency peaks at $20 < N_c < 30$, which can be used as a crude guide for the design of gyrotron oscillators. It will be shown in Section IV that N_c also serves as a useful parameter for determining the accessibility of the high efficiency regime.

3) The wave electric field $E_{\theta 0}$ at optimum efficiency operation is stronger for the tapered magnetic field case than for the constant magnetic field case because more beam energy has to be extracted in the former case to reach the higher efficiency (cf. Table I through VI). As a result, one gains the additional advantage of achieving higher wave power as well as higher efficiency by tapering the magnetic field. Near the peak efficiency, for example, QP_w for the tapered magnetic field is higher than that for the constant magnetic field by a factor > 2.

We conclude this section with a specific design example based data number 14 in Table III. To convert the normalized data quantities into physical design parameters, one needs to specify the desired wave frequency (f) and the quality factor Q. In the example, we shall let $f = 35$ GHz and $Q = 500$. The wall radius (r_w) is then given by

$$r_w = 4.775\,\bar{\omega}/f \text{ cm}$$

where f is in gigahertz. From Table III, we obtain $\bar{\omega} = 3.85$. Thus, $r_w = 0.526$ cm. In terms of r_w, the cavity length (L), the beam guiding center position (r_0), the magnetic field profile (B_1 and ΔB), and the wave electric field amplitude ($E_{\theta 0}$) can all be specified through the following formulas:

$$L = \bar{L} r_w \text{ cm}$$

$$r_0 = \bar{r}_0 r_w \text{ cm}$$

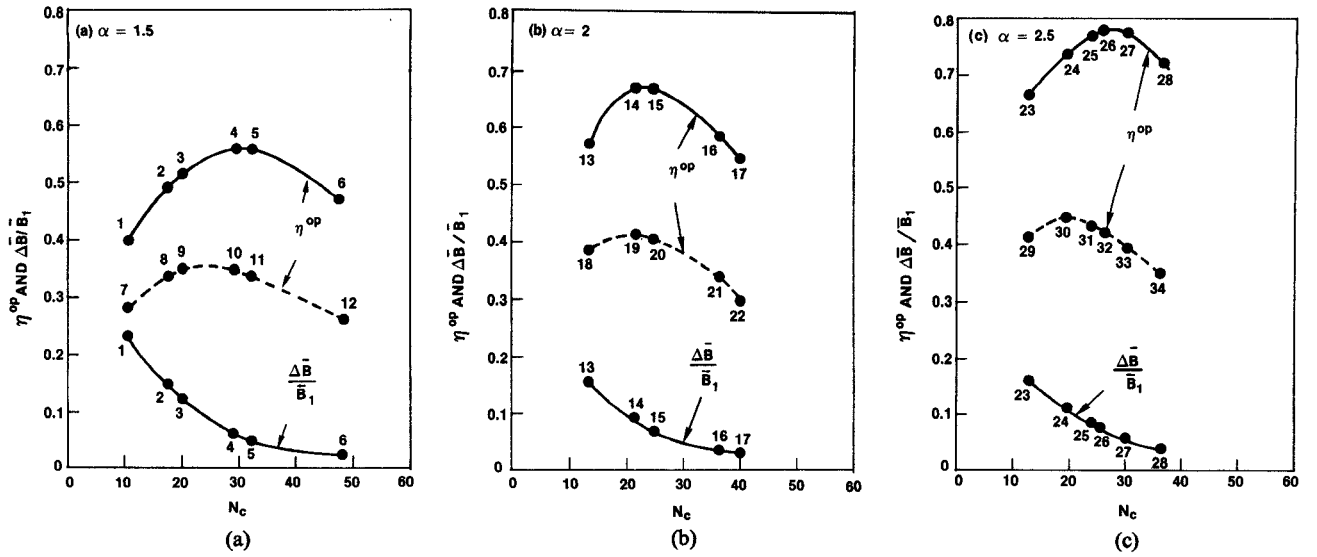

Fig. 3. η and $\Delta\bar{B}/\bar{B}_1$ versus N_c for (a) $\alpha=1.5$, (b) $\alpha=2$, and (c) $\alpha=2.5$. Solid and dashed curves refer to tapered and constant magnetic field profiles, respectively. Numbers associated with the dots refer to the data numbers shown in Tables I through VI.

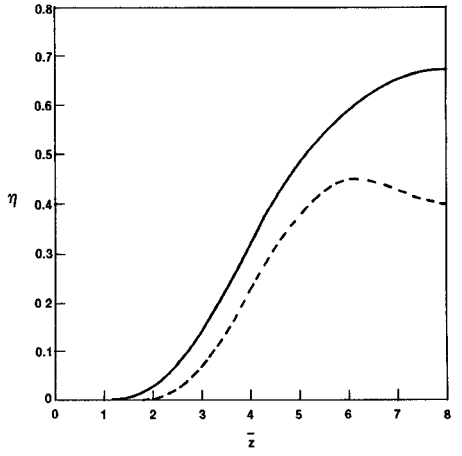

Fig. 4. η versus $\bar{z}$ for the TE_{011} mode, $\bar{L}=8$, and $\alpha=2$. Solid and dashed curves refer to the tapered and constant magnetic-field profiles, respectively.

$$\begin{Bmatrix} B_1 \\ \Delta B \end{Bmatrix} = 1.707 r_w^{-1} \begin{Bmatrix} \bar{B}_1 \\ \Delta\bar{B} \end{Bmatrix} \text{kG}$$

$$E_{\theta 0} = 512.1 r_w^{-1} \bar{E}_{\theta 0} \text{ kV/cm}$$

where r_w is in unit of cm. Finally, dividing QP_b^{th} and QP_b^{op} by Q gives, respectively, P_b^{th} and P_b^{op}. Table VII summarizes the parameters of the 35-GHz gyrotron oscillator design example.

IV. Accessibility of the High-Efficiency Regime

A comparison between the small signal theory of [17] and the present large signal theory shows that the optimum conditions for small and large signal interactions are close but not identical. Furthermore, the difference becomes more and more pronounced as N_c increases. As an example, we consider the following three cases involving a constant magnetic field (cf. data number 18, 19, and 20 in Table IV): (i) TE_{011} mode, $\bar{L}=5$, $N_c=13.4$, (ii) TE_{011} mode, $\bar{L}=8$, $N_c=21.5$, and (iii) TE_{021} mode, $\bar{L}=5$, $N_c=24.7$. As shown in Table IV, optimum efficiency operation requires a magnetic field ($\bar{B}_0$) of 4.126, 4.142, and 7.607 for cases (i), (ii), and (iii), respectively, while the small signal theory [17] predicts that strongest interaction occurs at $\bar{B}_0=4.242$, 4.276, and 7.855 for the same cases. Thus, optimum magnetic field in the small signal regime is higher than that in the larger signal regime by 2.8, 3.2, and 3.3 percent, respectively, for the three cases. This raises a question concerning the accessibility of the high efficiency (large signal) regime. Consider, for example, an experiment in which parameters are optimized for high efficiency operation. To reach the large signal operating regime, one has to first start from the small signal regime. But since the experimental parameters are not optimum for the transient small signal regime, the beam power required to start the small signal oscillation may be higher than the beam power (P_b^{op}) required for the large signal operation. As a result, the oscillation may not be started with the designed beam power P_b^{op}. This point is quantatively illustrated in Fig. 5 (a), (b), and (c), where QP_b and η for the three cases just considered are plotted against QP_w, a quantity proportional to the field energy in the cavity. In addition, the three corresponding cases (data number 13, 14, and 15 in Table III) involving tapered magnetic field are also plotted. Note that the magnetic fields used in obtaining Fig. 5 are those shown in Tables III and IV which are optimized for high efficiency rather than for small signal interaction. P_b in the limit of small cavity field ($P_w \to 0$) is defined as P_b^{th}, and P_b corresponding to the peak of η is referred to as P_b^{op}. For case (i)

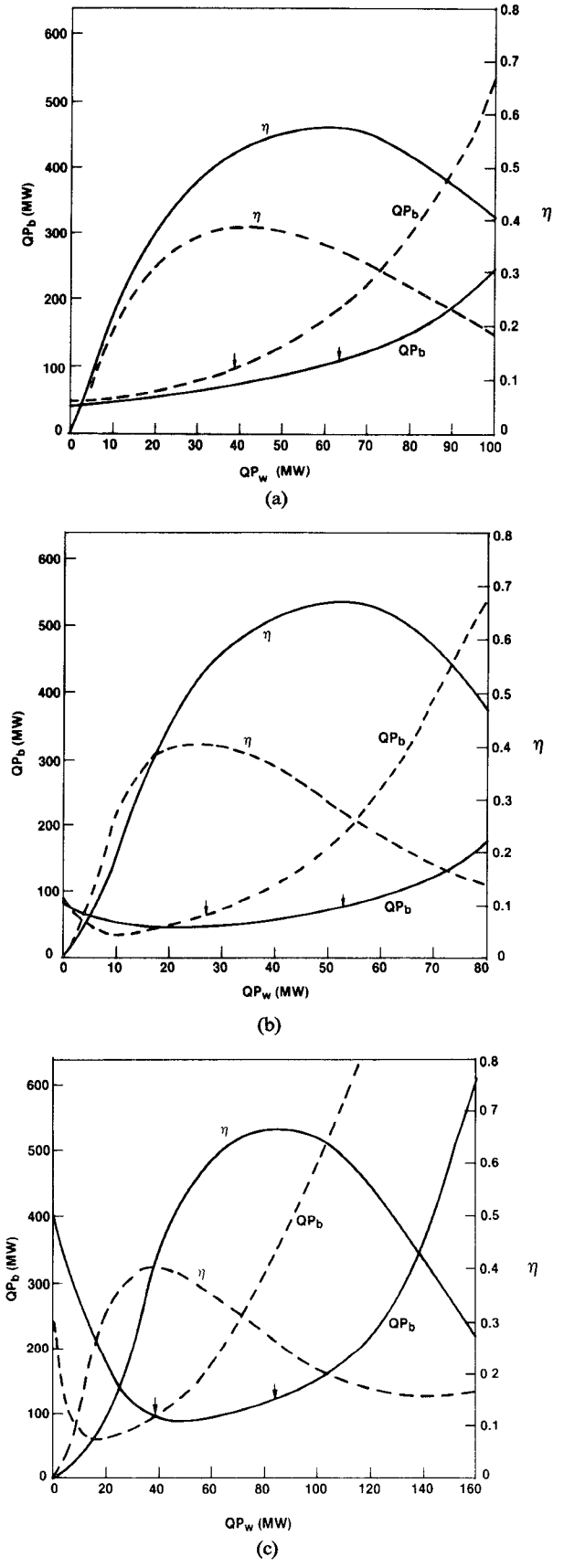

Fig. 5. QP_b and η versus QP_w for $\alpha=2$. Solid and dashed curves refer to the tapered and constant magnetic field profiles, respectively. QP_b at $QP_w=0$ gives the threshold beam power P_b^{th}. QP_b at the peak of η (marked by an arrow) gives the optimum beam power P_b^{op}. (a) TE_{011} mode, $\bar{L}=5$, $N_c=13.4$, (b) TE_{011} mode, $\bar{L}=8$, $N_c=21.5$, and (c) TE_{021} mode, $\bar{L}=5$, $N_c=24.7$.

where $N_c=13.5$, the difference between the optimum conditions for the small and large signal regimes is insignificant so that P_b^{th} is well below P_b^{op} and the large signal regime is easily accessible. For case (ii) where $N_c=21.5$, the difference becomes more pronounced such that P_b^{th} is comparable to P_b^{op}. Still, the oscillation can be started with a beam power slightly greater than P_b^{op}. For case (iii), however, the difference becomes so great that P_b^{th} is well above P_b^{op}. In which case, one of the following procedures would have to be taken to reach the high efficiency regime. 1) One initially operates with a beam power greater than P_b^{th} to build up the cavity field and later lower it to P_b^{op} to achieve high efficiency; 2) one initially operates in a higher magnetic field for which P_b^{th} is below P_b^{op} and slowly lowers it to the designed value after the oscillation has started; and 3) one builds up the cavity field with externally injected wave to the point where it can be further pumped up with P_b^{op} to reach the high efficiency regime. It is interesting to note that Kisel *et al.* [9] have used procedure 2) to reach their high efficiency operating regime. The present analysis provides a theoretical interpretation of their procedure. We note also that in more severe cases, the beam actually absorbs the field energy in the small signal regime when conditions are optimized for high efficiency. Such cases are indicated by $P_b^{th}=\infty$ in Tables I through VI.

V. Discussion

So far we have neglected the ohmic power loss on the cavity wall. The results could be easily modified to incorporate the effect of ohmic loss. In the presence of a resistive wall, a fraction of the extracted beam power will be dissipated in the wall as heat loss, the remaining fraction F comes out as wave power, where

$$F=Q_{ohm}/(Q_{ohm}+Q_d)$$

and Q_{ohm} and Q_d are, respectively, the ohmic and diffraction Q of the cavity as commonly defined. Thus, all the results remain valid provided that Q is now defined as $Q=Q_{ohm}Q_d/(Q_{ohm}+Q_d)$ and that the calculated values of P_w and η are multiplied by the factor F.

In our calculations, we have always positioned the electron beam on the peak of the electric field. This has allowed us to obtain the maximum efficiency with the minimum beam power. For some applications, however, higher wave power is desired. This can be achieved without sacrifice in efficiency by positioning the beam away from the peak of the electric field. In such a case, the optimum wave electric field as shown in Tables I through VI refers to the *local* field exerted on the electrons, and consequently the peak field is higher than that indicated in the Table, implying higher wave power and proportionally higher beam power under optimum operating conditions. For example, if the local electric field is half of the peak electric field, both the beam power and the wave power will be four times higher.

Here we have shown that a simple linearly tapered magnetic field (see Fig. 2) results in dramatic enhancement in efficiency. Although no calculations have been

made for a more complicated magnetic field profile, it appears likely that variations from the linear profile may result in further efficiency enhancement. It is also expected that the ultimate efficiency limit may very well be achieved by a combination of magnetic field and wave electric field contouring. All these possibilities point out that further research in this area is warranted and will almost certainly lead to even more efficient gyrotrons.

Experiments are being performed on the NRL gyrotron facilities to test the present theory. The initial design is based on data number 1 in Table I with $r_w = 0.53$ cm and $f = 35$ GHz. The magnetic field taper is produced by the addition of a shaped iron collar. Preliminary results indicate that the efficiency is increased from 28 to 37 percent as the magnetic field taper magnitude ($\Delta B/B_1$) is varied from 0 to 10 percent, in very good agreement with theoretical predictions. In this experiment, the operating parameters ($\Delta B/B_1$, L, α, etc.) were not yet optimized for maximum efficiency. Encouraged by the initial positive results, current effort is focused on parameter optimization so that much higher efficiency can be achieved.

Acknowledgment

The authors would like to thank Dr. P. Sprangle, Dr. V. L. Granatstein, and Dr. R. Smith for many stimulating discussions.

References

[1] K. R. Chu and J. L. Hirshfield, "Comparative study of the axial and azimuthal bunching mechanisms in electromagnetic cyclotron instabilities," *Phys. Fluids*, vol. 21, pp. 461–466, 1978.

[2] V. A. Flyagin, A. V. Gaponov, M. I. Petelin, and V. R. Yulpatov, "The gyrotron," *IEEE Trans. Microwave Theory Tech.*, vol. MTT-25, pp. 514–521, 1977.

[3] J. L. Hirshfield and V. L. Granatstein, "The electron cyclotron maser—An historical survey," *IEEE Trans. Microwave Theory Tech.*, vol. MTT-25, pp. 522–527, 1977.

[4] G. N. Rapoport, A. K. Nemak, and V. A. Zhurakhovskiy, "Interaction between helical electron beams and strong electromagnetic cavity-fields at cyclotron frequency harmonics," *Radio Eng. Electron. Phys.*, vol. 12, pp. 587–595, 1967.

[5] G. S. Nusinovich and R. E. Erm, *Elekron Tekh.*, Ser. 1, *Elektron.* SVCh, No. 2, p. 55, 1972.

[6] V. L. Bratman, M. A. Moiseev, M. I. Petelin, and R. E. Erm, "Theory of gyrotrons with a non-fixed structure of the high-frequency field," *Radiophys. Quantum Electron.* vol. 16, pp. 474–480, 1973.

[7] S. V. Kolosov and A. A. Kurayev, "Comparative analysis of the interaction at the first and second harmonics of the cyclotron frequency in gyroresonance devices," *Radio Eng. Electron. Phys.*, vol. 19, no. 10, pp. 65–73, 1974.

[8] A. A. Kurayev, F. G. Schevchenko, and V. P. Shestakovich, "Efficiently optimized output cavity profiles that provide a higher margin of gyroklystron stability," *Radio Eng. Electron, Phys.*, vol. 19, no. 5, pp. 96–103, 1974.

[9] D. V. Kisel, G. S. Korablev, V. G. Navel'yev, M. I. Petelin, and S. E. Tsimring, "An experimental study of a gyrotron, operating at the second harmonic of the cyclotron frequency, with optimized distribution of the high frequency field," *Radio Eng. Electron. Phys.*, vol. 19, pp. 95–100, Apr. 1974.

[10] A. V. Gaponov, A. L. Gol'denberg, D. P. Grigor'ev, T. B. Pankratova, M. I. Petelin and V. A. Flyagin, "Experimental Investigation of Centimeter Band Gyrotrons," *Radiophys. Quantum Electron.* vol. 18, no. 2, pp. 204–211, 1975.

[11] S. N. Vlasov, G. M. Zhislin, I. M. Orlova, M. I. Petelin, and G. G. Rogacheva, "Irregular waveguides as open resonators," *Radiophys. Quantum Electron*, vol. 12, no. 8, pp. 972–978, 1969.

[12] M. E. Read, R. M. Gilgenbach, A. J. Dudas, R. Lucey Jr., K. R. Chu, and V. L. Granatstein, "Operating characteristics of a 35 GHz gyromonotron," in *IEDM Tech. Dig.*, pp. 172–174, Dec. 1979.

[13] H. R. Jory, F. Friedlander, S. J. Hegii, J. R. Shively, and R. S. Symons, "Gyrotrons for higher power millimeter wave generation," in *IEDM Tech. Dig.*, pp. 234–237, Dec. 1977.

[14] Soviet work on contoured magnetic field has been briefly mentioned in [2, p. 579]. However, we have not been able to find the literature describing the details of their work.

[15] P. Sprangle and R. Smith, "The nonlinear theory of efficiency enhancement in the electron cyclotron maser," Naval Research Lab. Memo Rep. 3983 (to be published).

[16] M. Read and R. Lucey, "Study on the initial development of high power millimeter wave sonics," Naval Research Lab. Memo Rep. (unpublished).

[17] K. R. Chu "Theory of electron cyclotron maser interaction in a cavity at the harmonic frequencies," *Phys. Fluids*, vol. 21, pp. 2354–2364, 1978.

[18] P. Sprangle and A. T. Drobot, "The linear and self-consistent nonlinear theory of the electron cyclotron maser instability," *IEEE Trans. Microwave Theory Tech.*, vol. MTT-25, pp. 528–544, 1977.

[19] K. R. Chu and A. T. Drobot, "Theory and single wave simulation of the gyrotron travelling wave amplifier operating at cyclotron harmonics," Naval Research Lab. Memo Rep. 3788 (to be published).

[20] K. R. Chu, A. T. Drobot, H. H. Sze, and P. Sprangle, "Theory and simulation of the gyrotron traveling wave amplifier operating at cyclotron harmonics," this issue, pp. 313–317.

[21] J. A. Seftor, A. T. Drobot, and K. R. Chu, "An investigation of a magnetron injection gun suitable for use in cyclotron resonance masers," *IEEE Trans. Electron Devices* vol. ED-26, pp. 1609–1616, 1977.

[22] H. R. Jory and R. S. Symons, private communication.